Supporting Information

FRAGMENTATION OF POLYMER NANOCOMPOSITES: MODULATION BY DRY AND WET WEATHERING, FRACTIONATION, AND NANOMATERIAL FILLER

Richard Zepp,[a,†] Emmanuel Ruggiero,[b,†] Brad Acrey,[a,c] Mary J. B. Davis,[a,d],Changseok Han,[c,e,f] Hsin-Se Hsieh,[a,d] Klaus Vilsmeier,[b] Wendel Wohlleben,[b] and Endalkachew Sahle-Demessie[e,] *

* Corresponding author

E-mail address: Sahle-Demessie.Endalkachew@epa.gov

† these authors contributed equally to this work

[a] U.S. Environmental Protection Agency (EPA), Office of Research and Development (ORD), Center for Environmental Measurement and Modeling (CEMM), 960 College Station Rd., Athens, GA, USA
[b] BASF SE, Dept. Material Physics and Analytics, 67056, Ludwigshafen, Germany
[c] ORISE Research Fellow
[d] NRC Post-Doctoral Fellow
[e] EPA, ORD, Center for Environmental Solutions and Emergency Response (CESER), Cincinnati, OH, USA
[f] Department of Environmental Engineering, INHA University, Incheon, Korea

# of pages **17**

# of Figures 15 and # Tables **1**

Environmental aging of polymer nanocomposites

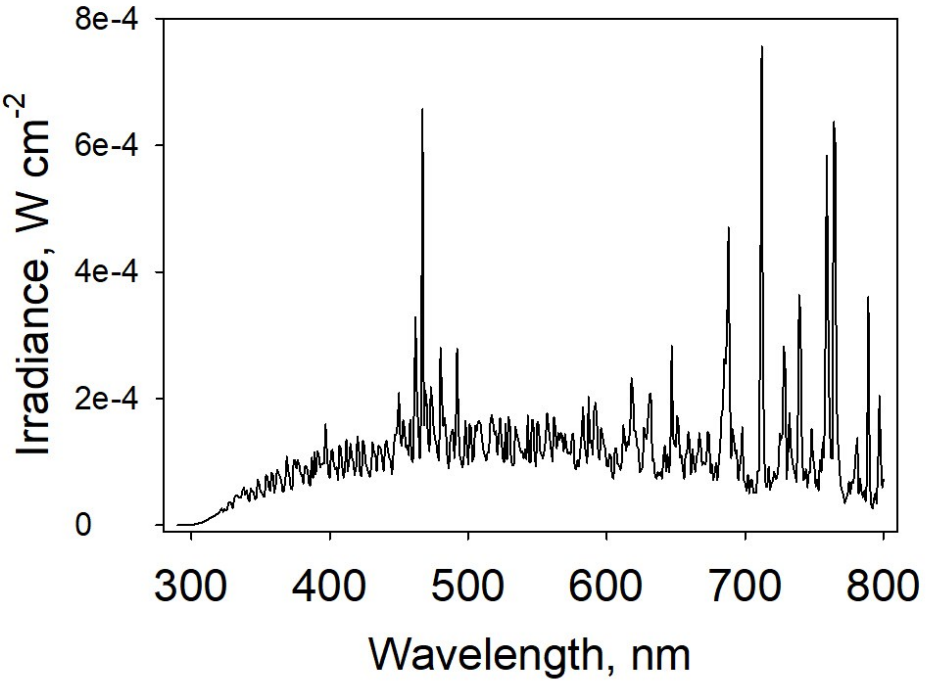

Figure S1. Spectral irradiance of XLS+ spectroradiometer used for weathering studies (irradiance negligible <295 nm). Measured using an Optronics OL-756 spectroradiometer.

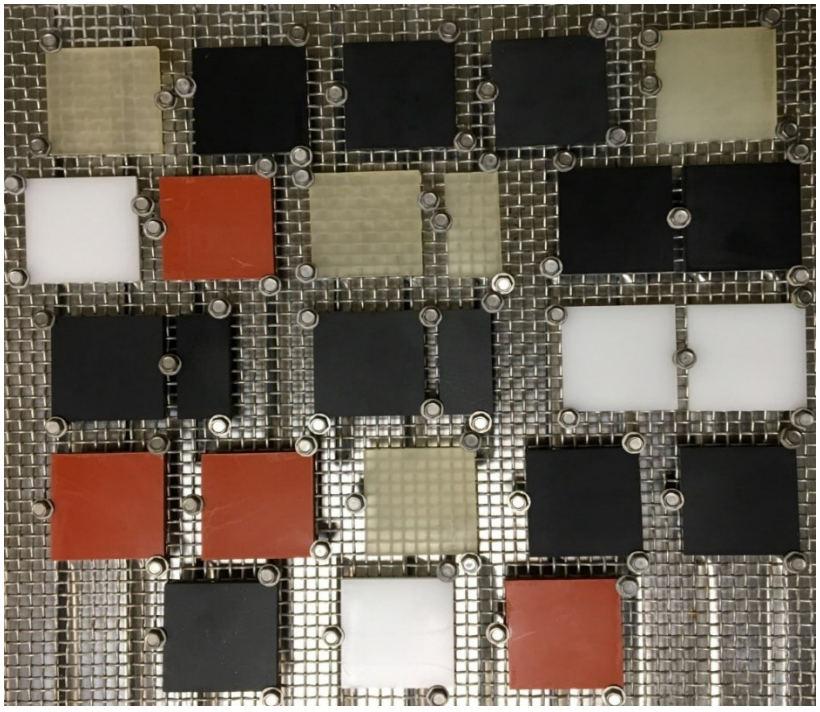

Figure S2. Sample wafer configuration inside weathering chamber showing randomization of wafer placement. Wafer reported are: transparent yellowish sample = unfilled epoxy wafer, black sample = carbonaceous filled epoxy wafer, white sample = unfilled PP wafer, reddish sample = Fe_2O_3 filled PP wafer.

Additional Characterization Techniques

Analytical Ultracentrifugation-Refractive Index detection (AUC-RI)

Analytical Ultracentrifugation (AUC) was performed on leaching water containing released fragments and nanoparticles using an AUC-Beckman XL centrifuge at 8000 rpm equipped with an interference optical system. For all NEPs, duplicate samples were prepared and measured for each experimental setup (e.g. dry vs wet, fractionated vs non-fractionated). A detailed description of AUC-RI was previously reported [1,2] and here quickly described. A refractive index detector was synchronized to the rotation of the centrifuge, to enable observation of the colloidal speed of migration during centrifugal separation. This AUC-RI technique allows for the quantitative detection of graphene, carbon black, and MWCNT traces to 1 ppm.[1] The method enables quantitative detection with size and concentration accuracy better than a 10%.[2] We reported the average size and the mass concentration observed in size range 5 nm to 1000 nm (which is based on observation during fractionation). The size detection interval by AUC can be quantitatively compared to the fractionation step introduced here for UV-vis analysis. For the typical dimensions of a preparative swing-out rotor (radius of liquid approx. 110 mm from rotational axis, filling of few mL resulting in liquid height of approx. 30mm), and for the typical density of polymer fragments (around 1.2 g/cm³), the operational parameters of 1000 rpm and 60 minutes correspond to a cut at 1µm: Particles above 1µm diameter are quantitatively removed from the suspension, such that the UV-vis analysis after fractionation observes the sub-micron fraction, in analogy to the detection interval of AUC from 1nm to about 1µm.

Only leachates subjected to the fractionation protocol were evaluated in order to reduce the presence of large wafer debris. Figure S3 shows the concentration (mg/ml) of released fragments from the different specimens. As in Figure 5, the unaged wafers have generally less emission of particles than the weathered ones. Apart from the case of epoxy graphene dry aged, the presence of the nanofiller reduced unspecifically the release of debris.

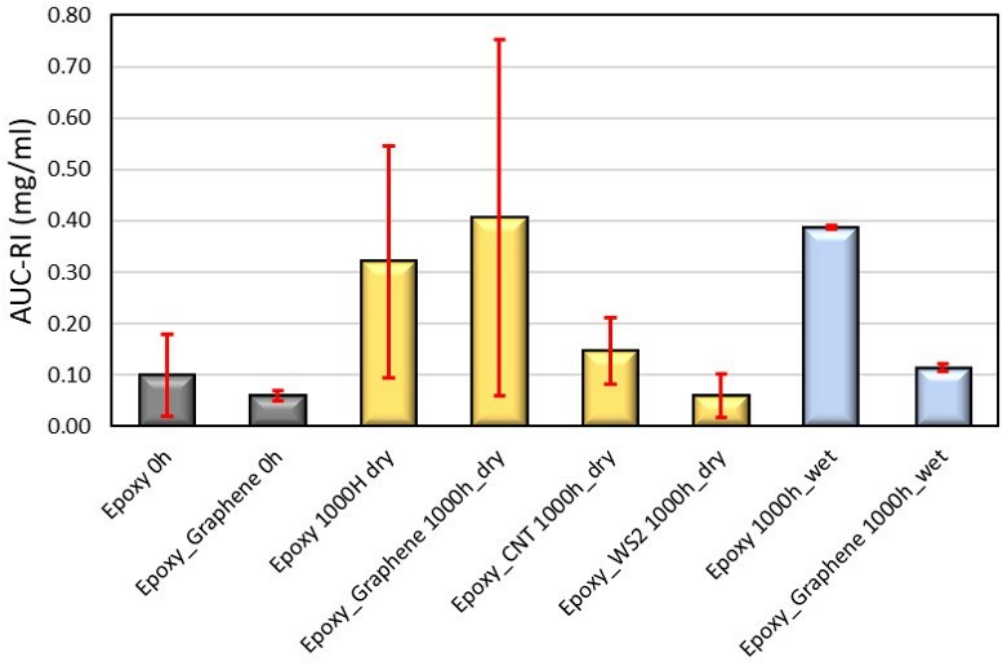

Figure S3. Results of analytical ultracentrifugation given as release in mg/ml from unaged (grey), 1000 h aged in dry condition (yellow) and 1000h aged in wet conditions (blue) materials.

In both UV and AUC bar graphs (Figure 5, S3 and S10a), Epoxy CNT composite differed in the form and rate of release: it generated larger fragments, as inferred from the fractionation losses, resisted differently to leaching and retarded the overall release. This is consistent with the working hypothesis that upon polymer degradation the remaining CNTs collapse to a dense entangled network, which blocks UV light and mechanically resists release[3-6]. On PU it was found that the equally black CB has less of a photoprotective effect than CNT.[7] Our present results confirm this also for epoxy matrix, and additionally find that stiff black fibers (WS2) or black waferlets (GP) or black particles (CB) can all not always reproduce the unique photoprotective effects of entangled black fibers (CNTs). The lack of UV absorption by SiO_2 does not seem to play a significant role with the present epoxy matrix.

Attempts at release quantification by Inductively Coupled Plasma-Mass Spectrometry (ICP-MS)

ICP-MS was performed at U.S. Environmental Protection Agency/ CESER-Cincinnati (EPA-CESER), and at U.S. Environmental Protection Agency/ CEMM, Athens (EPA-CEMM)

using a Perkin Elmer NexION 300D ICP-MS with an ESI SeaFAST autosampler (PerkinElmer Inc, CT, USA Similar digestion procedure was followed as in [8], where method 3050B was used as referenced. The following metals were analyzed and reported in concentrations of ppm: Co, Fe, Ni, Cr, Al, Ca, Mg, Mn, Ti, and Si. Minimum reporting limits (MRL) for samples analyzed range from 5 ppb for Nickel to 1000 ppb for Ca.

ICP-MS characterization and quantification proved difficult in this set of experiments, as there were no results with statistical significance, with the exception of ~2.5 folds increase of nickel in dark vs. 1000 hour weathered epoxy-carbon black (20 ppb to 50 ppb). All other elemental mass observations either stayed the same or decreased over the course of weathering or were significantly less than that of our control samples, as was the case in most of our study. There was also an issue of detection limit with silicon, as well as being a hard element to quantify with possible sources of contamination within the laboratory.

Attempts at particle sizing by dynamic light scattering (DLS, Zetasizer, Malvern Panalytica)

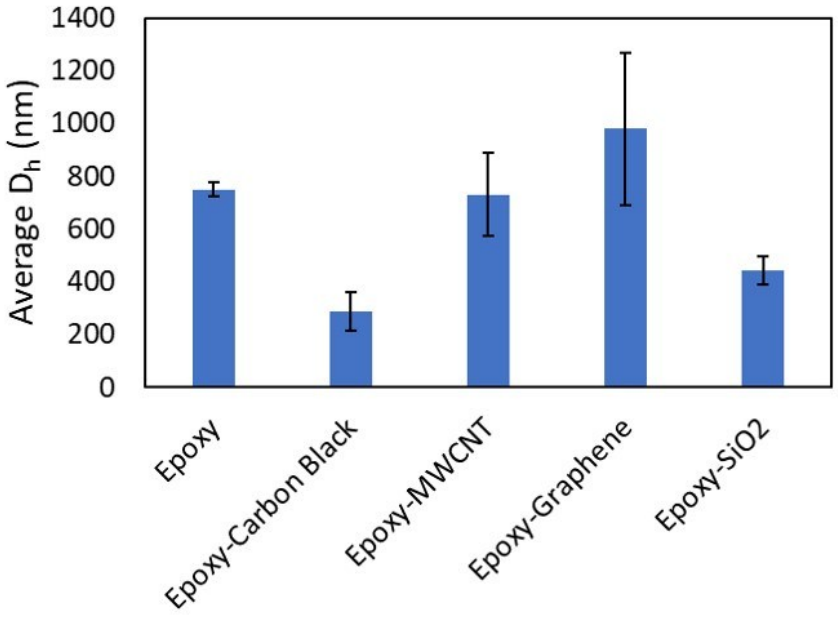

Figure S4. Dynamic Light Scattering plot for Epoxy and Epoxy-ENM's. Note: Polydispersity Index was too high (> 0.6) for Epoxy, Epoxy-MWCNT, and Epoxy-Graphene to make an accurate determination of particle size.

Chemical and Physical Changes in Weathered Wafers

Attenuated Total reflectance Fourier transform infrared spectroscopy (ATR-FTIR)

Carbonyl index (CI), was used as a parameter to monitor the degree of photo-oxidation of epoxy and has been calculated according to the baseline method [9] to the absorbance of the strong peak due to the asymmetric C-H stretching at 1465 cm^{-1} [10]. Carbonyl index is the ratio between the absorbance of the carbonyl peak (1712 cm^{-1}) and the absorbance of the -CH_2 groups at 1465 cm^{-1}.

$$Carbonyl\ Index\ (CI) = \frac{Absorption\ at\ 1712\ cm^{-1}}{Absorption\ at\ 1465\ cm^{-1}} \quad \text{.....(S1)}$$

The CI is given at the ratio of the maximum absorption carbonyl peak and a peak for an unreactive peak in the ATR-FTIR spectrum.

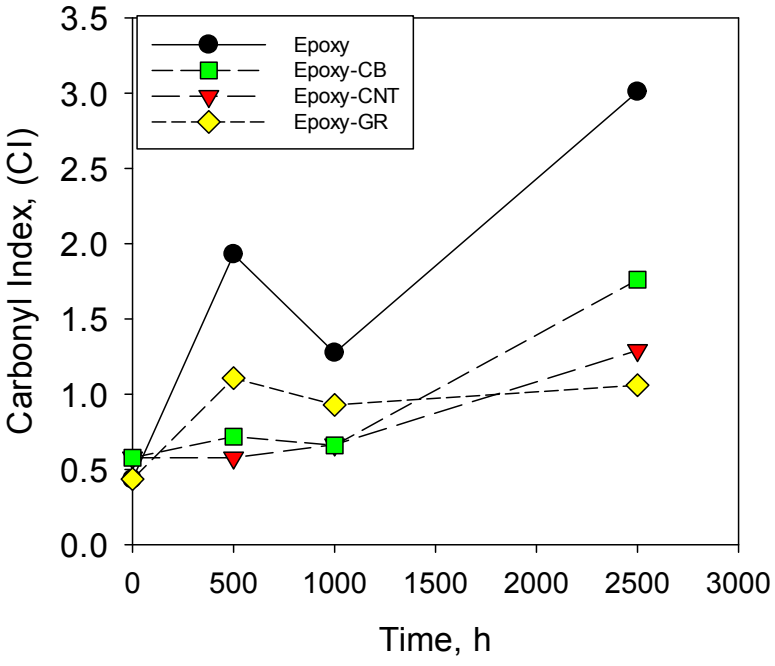

a

Figure S5. Ratio of ATR-FTIR spectra peak intensities at 1712 cm-1 (characteristic peak of C=O in saturated aldehyde, ketone or acid)

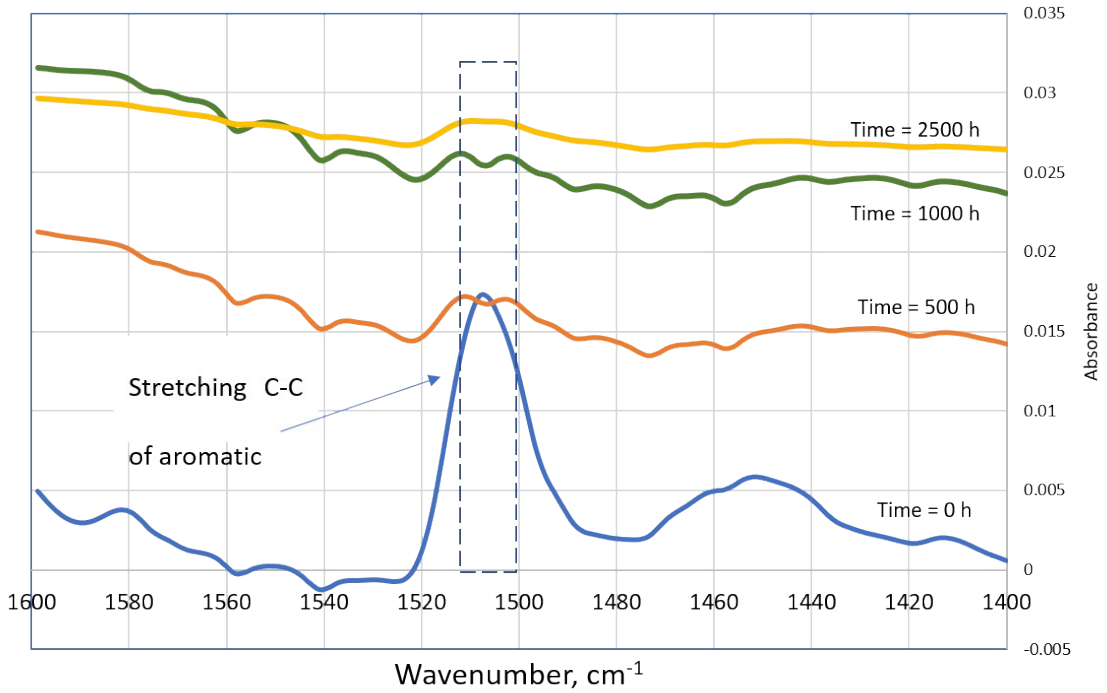

Figure S6. Section of FTIR spectra of epoxy-graphene with different aging times showing the decrease in the peak absorbance for stretching C-C of aromatics of epoxy.

Mass and Thickness Loss of Weathered Wafers

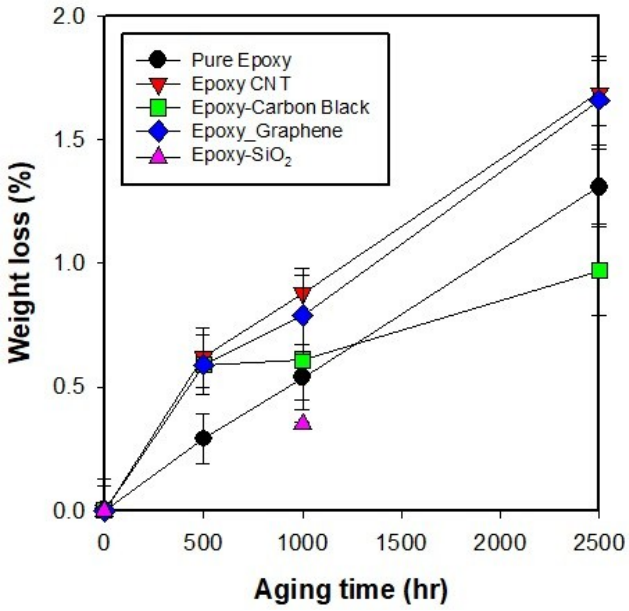

Figure S7. Mass loss upon wet weathering of epoxy and epoxy composites. Masses measured at corresponding time intervals on a microbalance and wafer thicknesses were measured using a micrometer. The error bars reflect multiple measurements on the same specimen performed only at EPA-CESER.

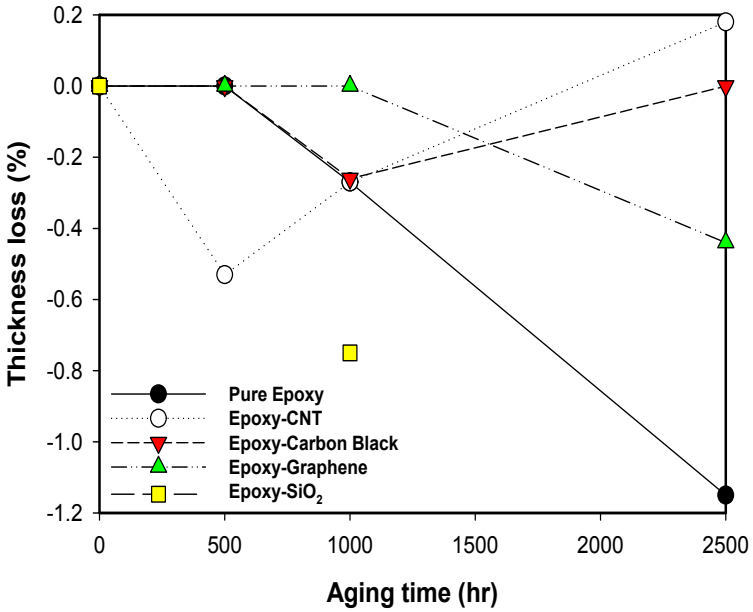

Figure S8. Thickness loss (right) for Epoxy and Epoxy-ENM samples as a function of aging time under wet conditions.

SEM and EDX Characterization of Selected Polymer nanocomposites

Scanning electron microscopy is an excellent tool to characterize changes occuring at or near the surface of materials. When coupled with an Energy Dispersive X-Ray (EDX) analyzer, the ability to assess elemental composition at relative sites on the surface can be emphasized. In Figure S9, EDX spectral data for two specific polymer nanocomposites obtained at EPA-CEMM are shown. Figure S9 (A) shows the weathered surface of an Epoxy-SiO_2 wafer in the top image, and the corresponding EDX spectrum below. There is a significant amount of Si that has accumulated at the surface. In the case of weathered Polyamide-Kaolin (Figure S9(B)), both Si and Al are detected at high levels, confirming the presence of Kaolin.

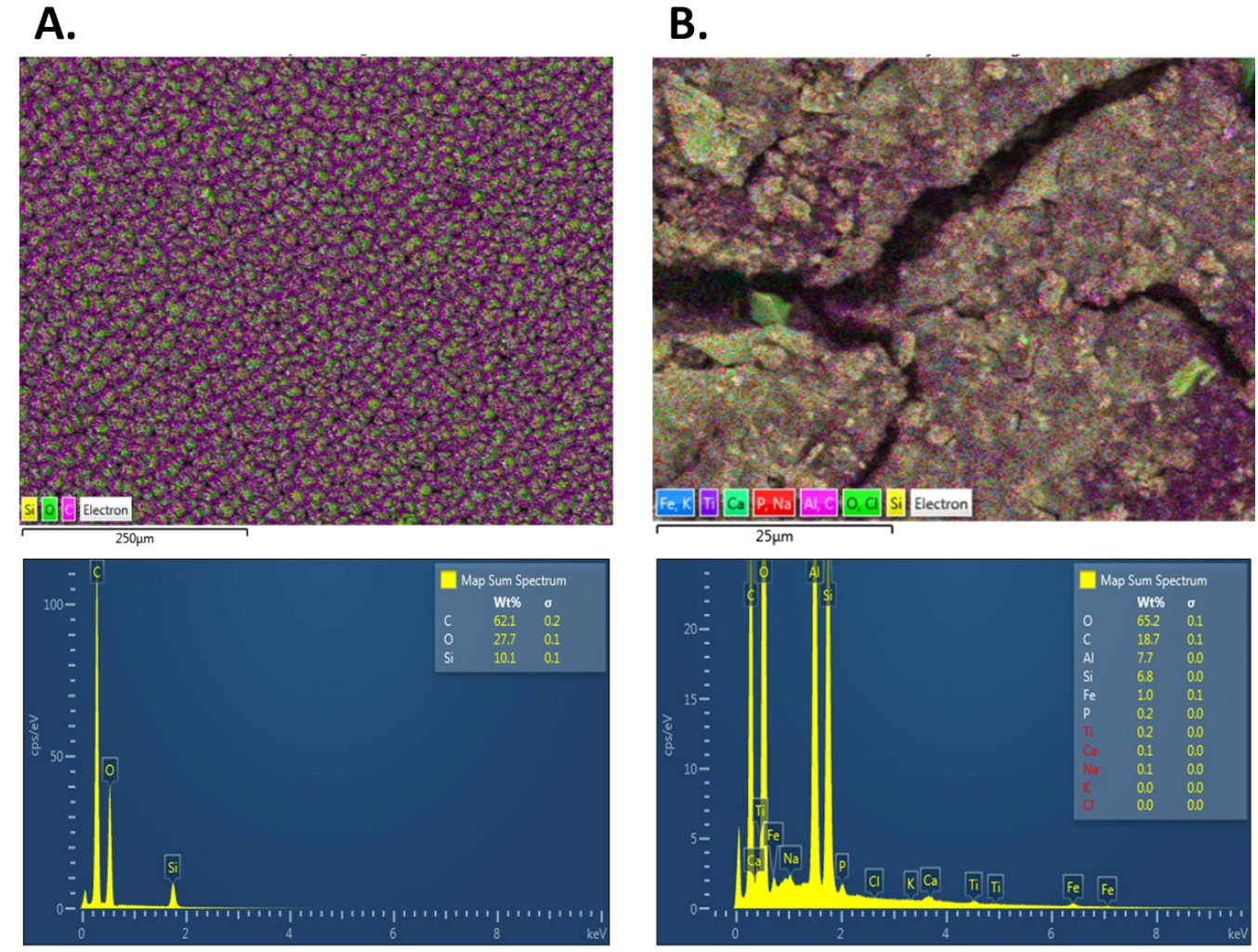

Figure S9. SEM and EDX (Energy Dispersive X-ray) analysis of Epoxy-SiO_2 (A) and Polyamide-Kaolin (B)

Quantification and Characterization of Released Fragments

Impacts of fractionation on quantification of release (see 3.5 main)

In this section we examine the variation of relative standard deviation (RSD) of UV leachate samples to evaluate how much data are clustered close to the mean value. RSD is calculated by dividing the standard deviation of a group of values by the average of the values. Higher values of RSD indicate data are more spread out and measurements are less precise. We considered the absorption coefficients between fractionated and non-fractionated samples

($\Delta(RSD_{Frac}\text{-}RSD_{No\text{-}Frac})$, Table S1) for Epoxy and PA wafers. All data considered derive from measurements performed at BASF and EPA-CEMM.

Regarding Epoxy wafers, we could observe for 6 samples out of 11 a negligible change (ΔRSD less than 5%). At the same time, 4 specimens had an intensive reduction of the $\Delta(RSD_{Frac}\text{-}RSD_{No\text{-}Frac})$ among the -9.4 and -38%. Only one sample (Epoxy Carbon Black_1000H_wet) had an increase of the delta of 27%.

At the same time, $\Delta(RSD_{Frac}\text{-}RSD_{No\text{-}Frac})$ of PA wafers present a more fluctuating trend. The delta ranges between a positive + 27.4 % and a negative -76.8%. However, in 4 cases out of 7 the fractionation step reduced the $\Delta(RSD_{Frac}\text{-}RSD_{No\text{-}Frac})$ among the -6.3 and -76.8%.

The comparison between the relative standard deviation (RSD) of non-fractionated and fractionated samples show that fractionation values are more often close to the group average. This demonstrates that the fractionation step improves the reproducibility of the outcomes.

Table S1: Relative standard deviation values of fractionated and non-fractionated samples

Sample	RSD_{Frac}	$RSD_{No\text{-}Frac}$	$\Delta(RSD_{Frac}\text{-}RSD_{No\text{-}Frac})$
Epoxy_1000H_dry	6.3	5.1	*+ 1.2 %*
Epoxy_WS2_1000H_dry	9.0	6.8	*+ 2.2 %*
Epoxy_CNT_1000H_wet	11.1	17.8	*+ 2.2 %*
Epoxy_1000H_wet	17.1	12.3	*+ 4.8 %*
Epoxy_Graphene_1000H_wet	20.8	22.9	*- 2.0 %*
Epoxy_CNT_1000H_dry	2.5	7.4	*- 4.9 %*
Epoxy_Graphene_1000H_dry	3.4	12.8	- 9.4 %
Epoxy_0H	53.2	71.2	- 18.0 %
Epoxy_Graphene_0h	43.0	81.0	- 38.0 %
Epoxy_SiO2_1000H_wet	19.1	42.1	- 23.0 %
Epoxy_Carbon Black_1000H_wet	68.3	40.9	+ 27.4 %
PA_2500h_wet	7.44	16.40	+ 9.0 %
PA_Kaolin_2500h_wet	59.12	73.16	+ 14.0 %
PA_0h	17.56	37.80	+ 20.2 %
PA_Kaolin_1000h_dry	10.10	3.82	- 6.3 %
PA_Kaolin_1000h_wet	75.42	47.14	- 28.3 %
PA_Kaolin_2500h_dry	72.91	1.79	- 71.1 %
PA_Kaolin_0h_dry	104.26	27.50	- 76.8 %

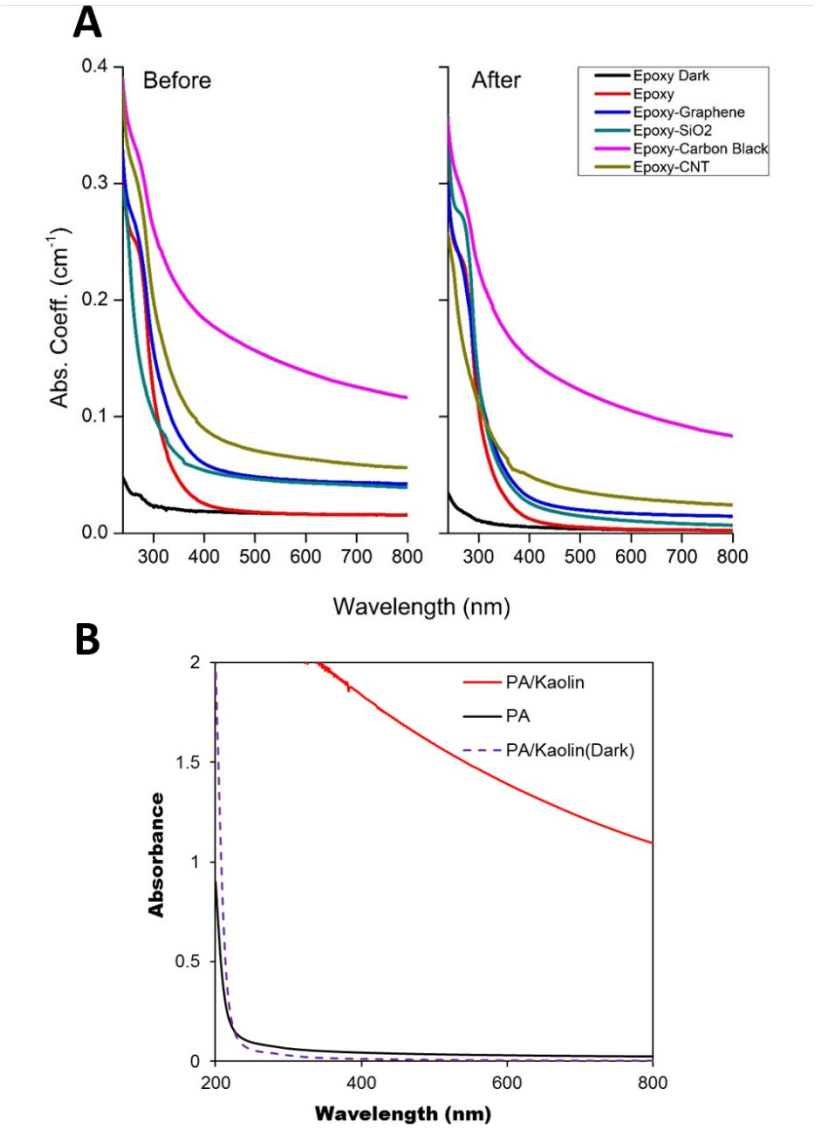

Figure S10. (A) UV-Vis spectra of non-fractionated (left) and fractionated (right) particles released from neat and composite epoxy wafers, suspended in water with 0.1% SDS (EPA-CEMM). The wafers were weathered using the wet aging method described in Section 2.3 (main), then collected as described in 2.6 (main) (B) UV-Vis spectra plots of non-fractionated leachate of PA samples.

Inter-laboratory comparison of nano-release using UV-Vis spectra data

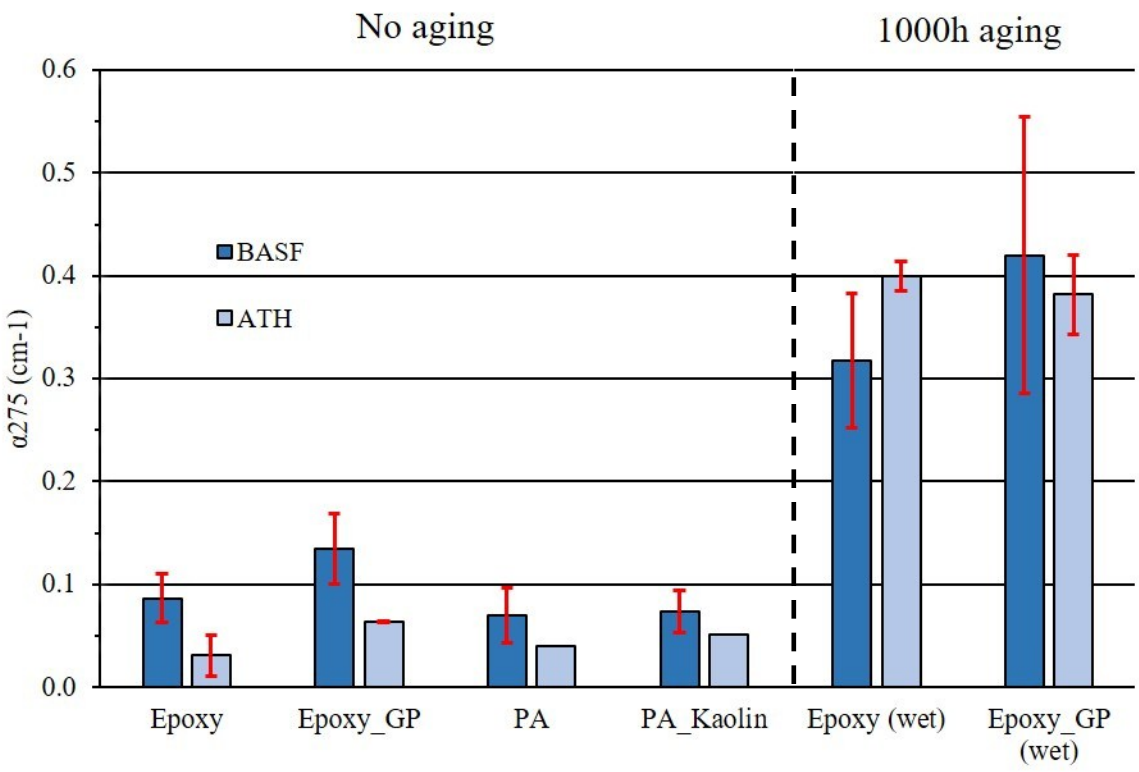

Figure S11. Comparison of absorption coefficients at 275 nm (α_{275}) of leaching fluid from wet-aged samples after fractionation between BASF (dark blue) and EPA-CEMM (light blue) shows good agreement between laboratories

Calculation of mass release and absorption coefficient rate

Mass release rate and absorption coefficient rate of the different leaching samples were respectively calculated taking in consideration all sampling-related parameters such as the wafer surface area, bubbling reduction and wafer immersion volume. These last two aspects were condensed in one factor: fragment dilution volume which permits to compare the results from the different labs. The equations employed are the following:

$$Mass\ release\ rate\left(\frac{mg}{MJ}\right) = \frac{fragment\ conc\ (\frac{mg}{m^3})}{energy\ dose\ (\frac{MJ}{m^2})} * \frac{fragment\ dilution\ volume\ (m^3)}{plate\ surface\ area\ (m^2)}$$

$$Abs\ coef\ rate\left(\frac{1}{\frac{MJ}{m^2}}\right) =$$

$$\frac{Abs}{pathlength\ (m)} * \frac{}{energy\ dose\left(\frac{MJ}{m^2}\right)} * \frac{fragment\ dilution\ volume\ (m^3)}{plate\ surface\ area\ (m^2)}$$

Cross-sectional TEM

Ultra-thin samples (~100 nm) for Transmission Electron Microscopy (TEM) were prepared by cryo-ultramicrotomy at temperatures of about -120 °C (Ultracut S; Leica Microsystems, Buffalo Grove, USA) and analyzed on a Libra 120 microscope (Carl Zeiss Microscopy GmbH, Jena, Germany) operated at 120 keV partly in energy-filtered mode (Ω-filter; inelastically scattered electrons). Images were evaluated using the Olympus (Tokyo, Japan) iTEM 5.2 (Build 3554) software package.

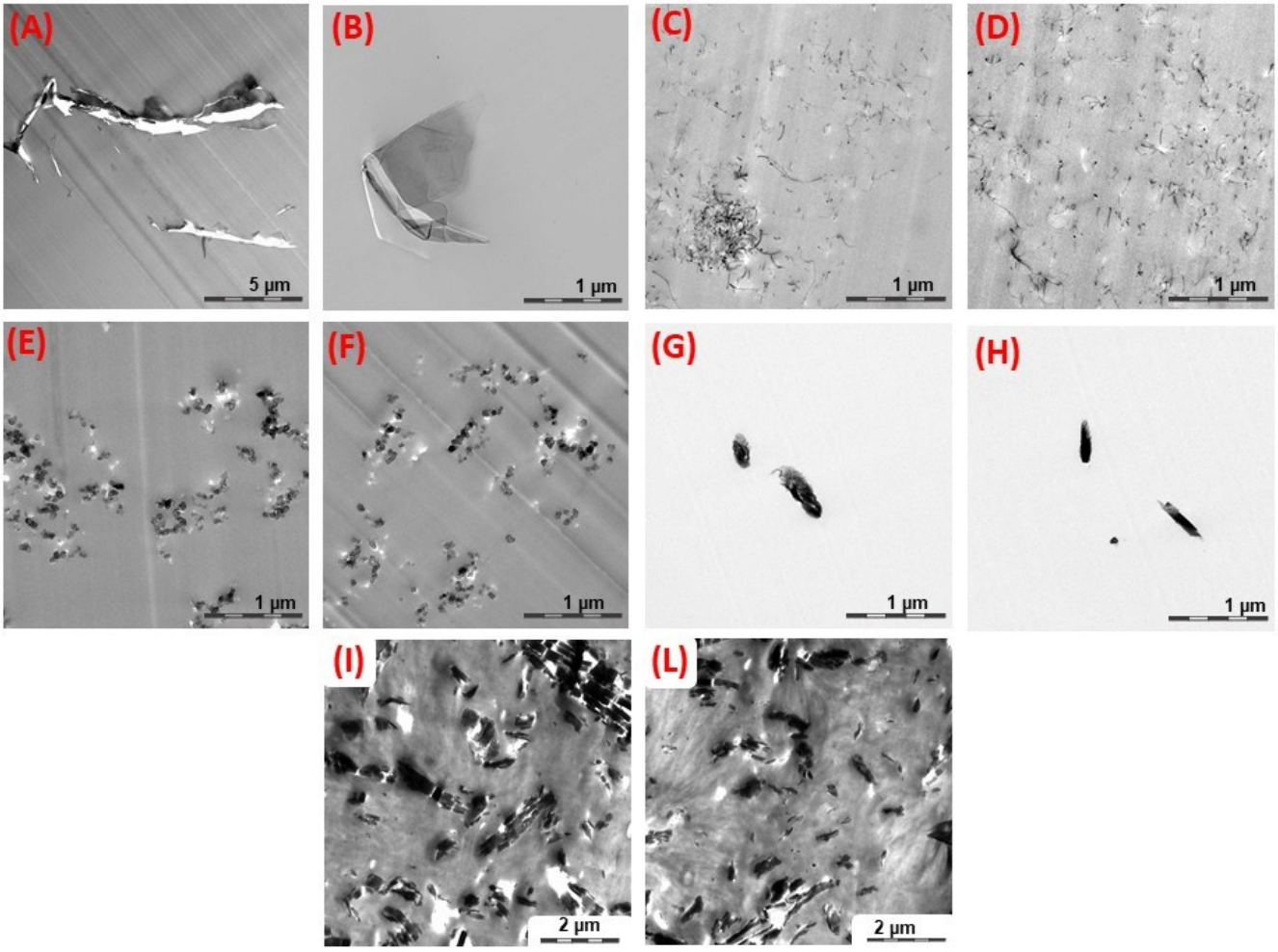

Figure S12: Cross-sectional transmission electron microscope images of nano-filled wafers (A, B) epoxy-graphene, (C, D) epoxy-CNT, (E, F) epoxy-CB, (G, H) epoxy-WS_2 and (I, L) PA-kaolin.

TEM-SAED (Selected Area Electron Diffraction)

The crystallinity of the samples was investigated by selected area electron diffraction (SAED) at 300mm camera length. The central beam was blanked. Images and diffraction patterns were evaluated using the iTEM (Olympus, Tokyo, Japan, version: 5.2.3554), Prodas (Proscope, Gangelt, Germany, version: 1.4) und TIA (FEI, version: 4.1.202) software packages.

SAED analysis confirmed the nature of the nanomaterial showing the typical hexagonal diffraction pattern. Fig S9-B displays an electron pattern originated from a single crystallite. The diffraction intensities were partially blurred out because the graphene sheets were not completely plane. Conversely, in Fig S9-D different crystal structures produced the SAED pattern. One larger crystallite produces the more intense diffraction, while the other patterns were generated from smaller crystals which were rotated in respect to the large one.

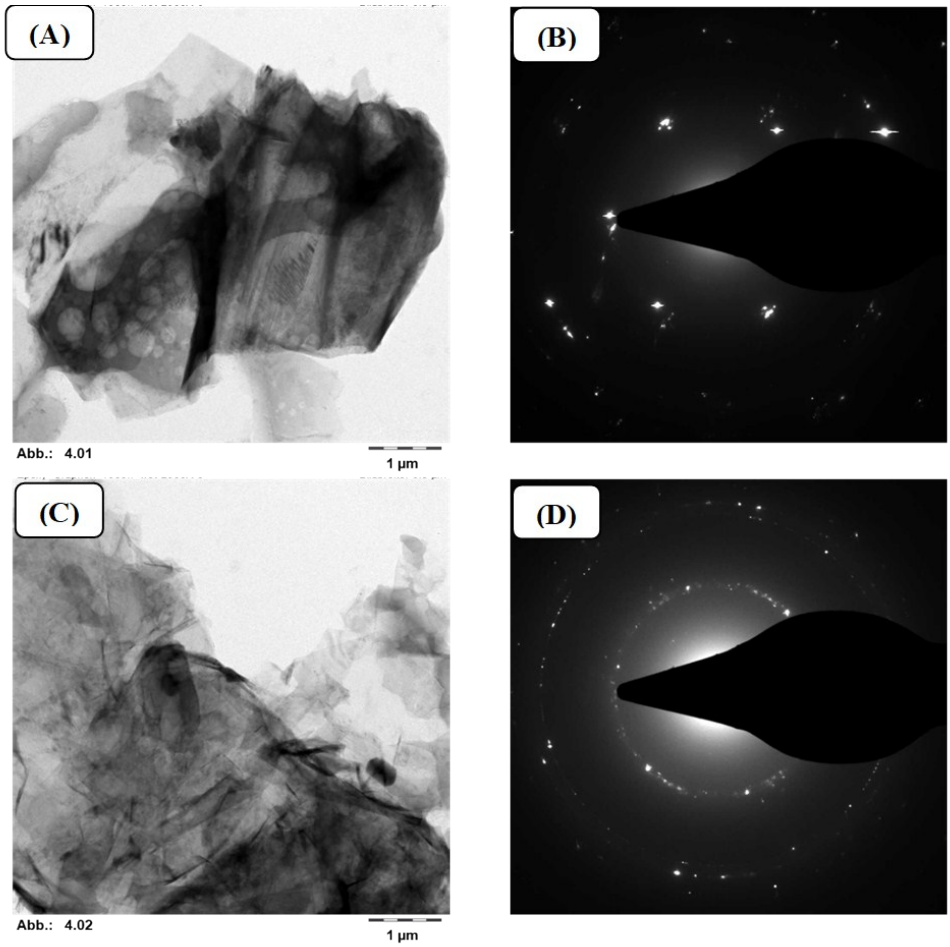

Figure S13. (A, C) TEM images and relative (B, D) SAED pattern showing graphene sheets released from epoxy wafers after 1000 h of aging.

TEM Imaging of released fragments

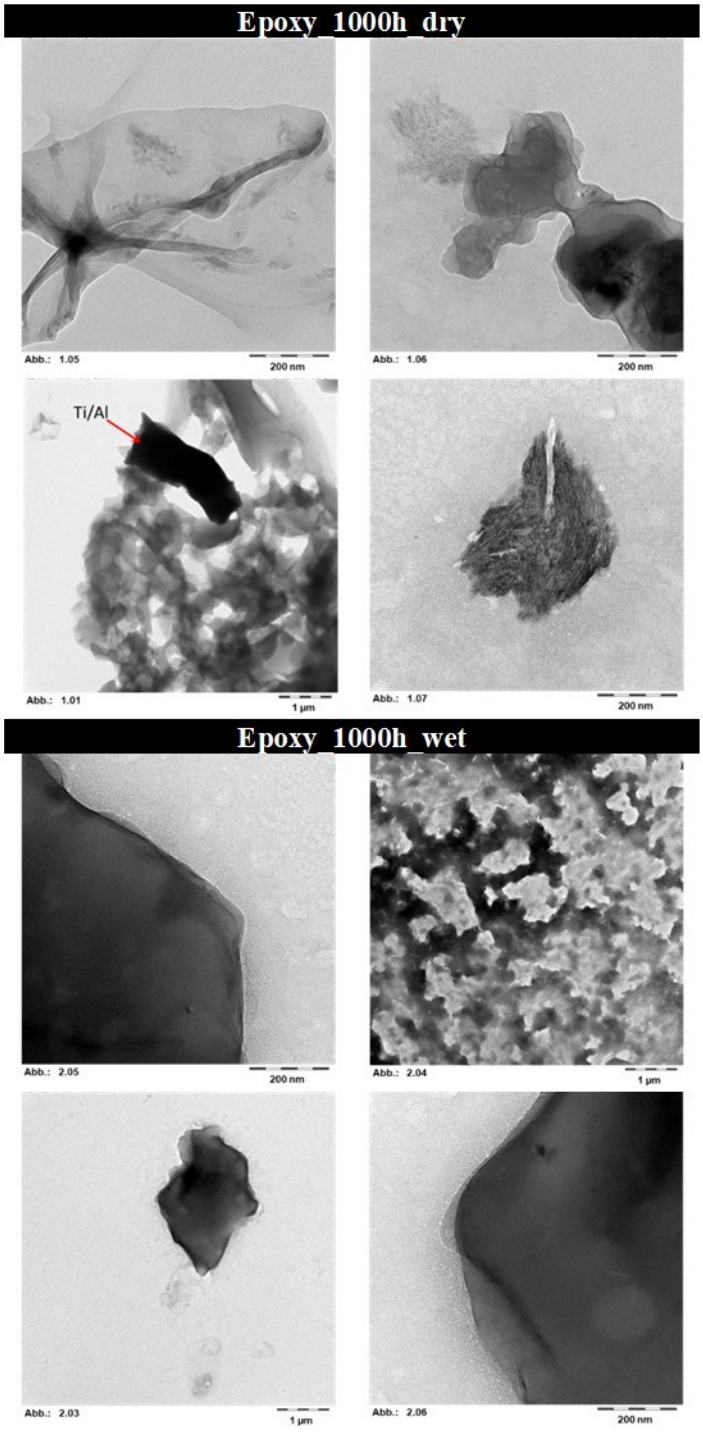

Figure S14. TEM pictures of emitted debris from 1000 h weathered epoxy wafers under (upper) dry and wet (down) conditions after fractionation step.

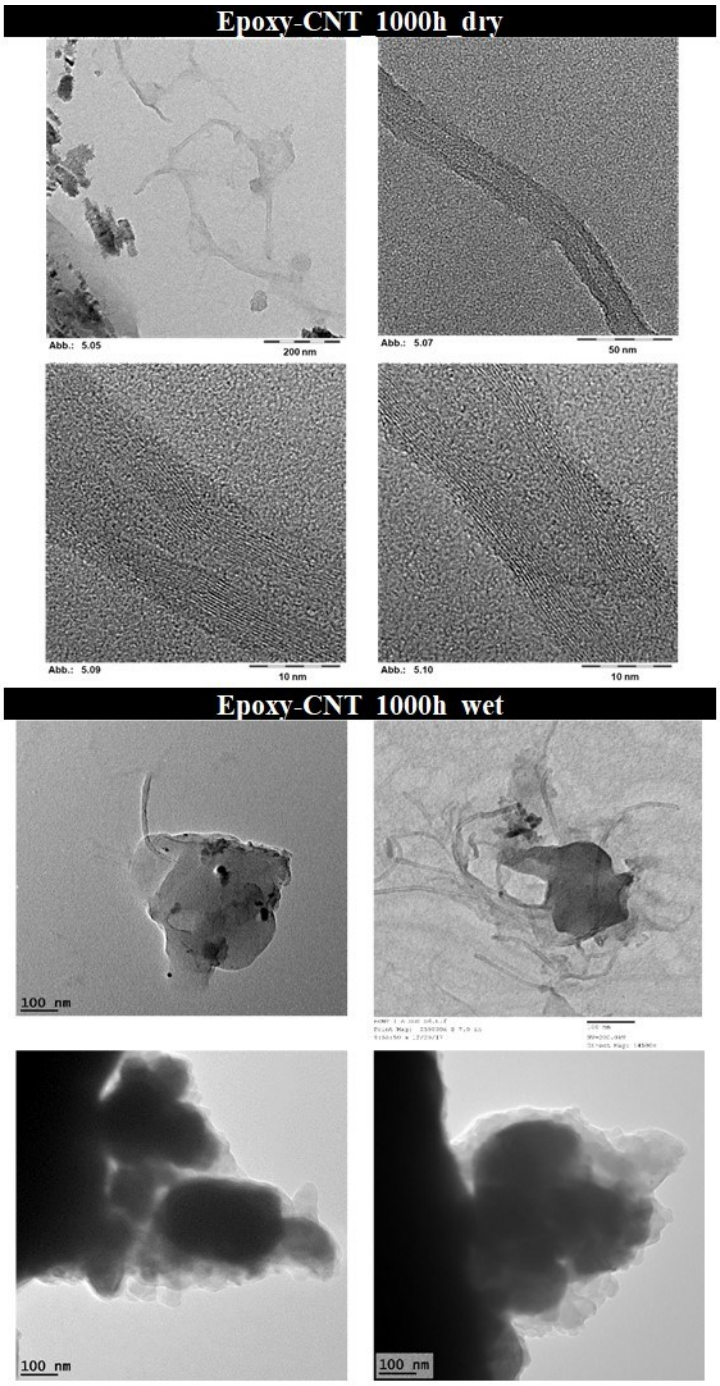

Figure S15. TEM pictures of emitted debris from 1000 h weathered epoxy-CNT wafers under (upper) dry and wet (down) conditions.

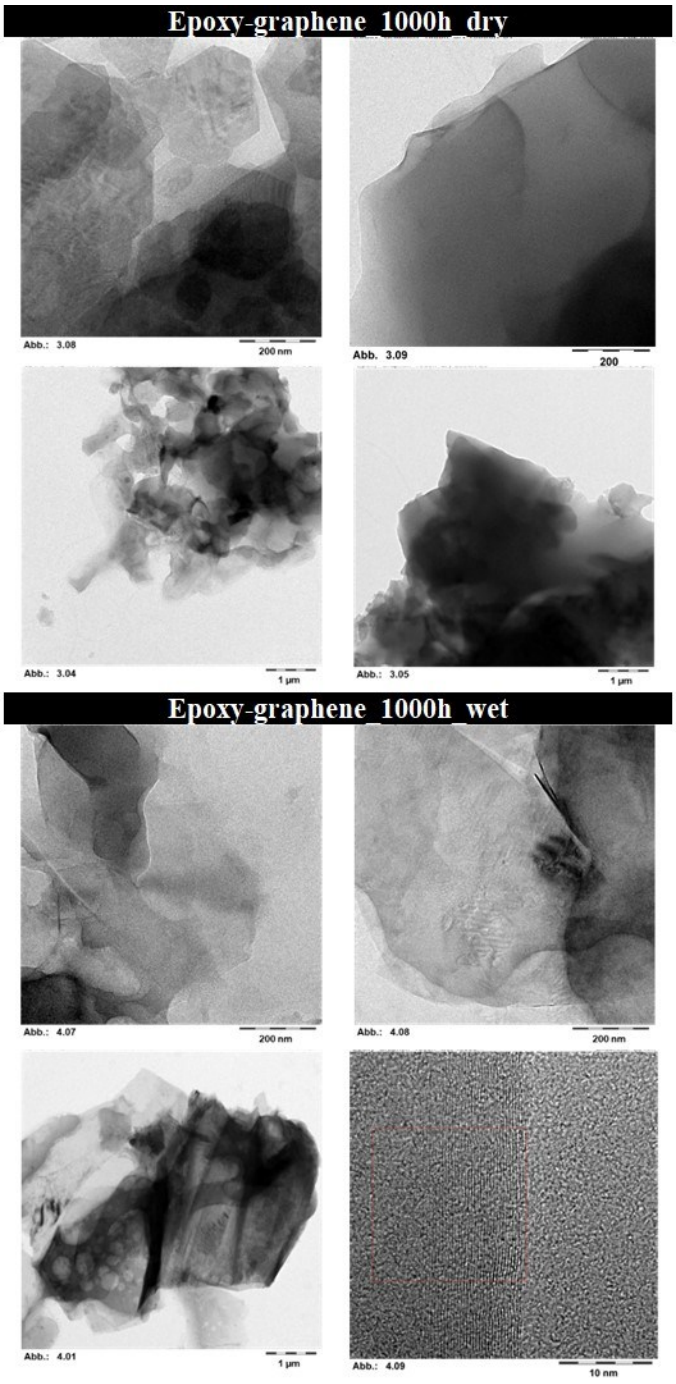

Figure S16. TEM pictures of emitted debris from 1000 h weathered epoxy-graphene wafers under (upper) dry and wet (down) conditions.

Raman spectroscopy

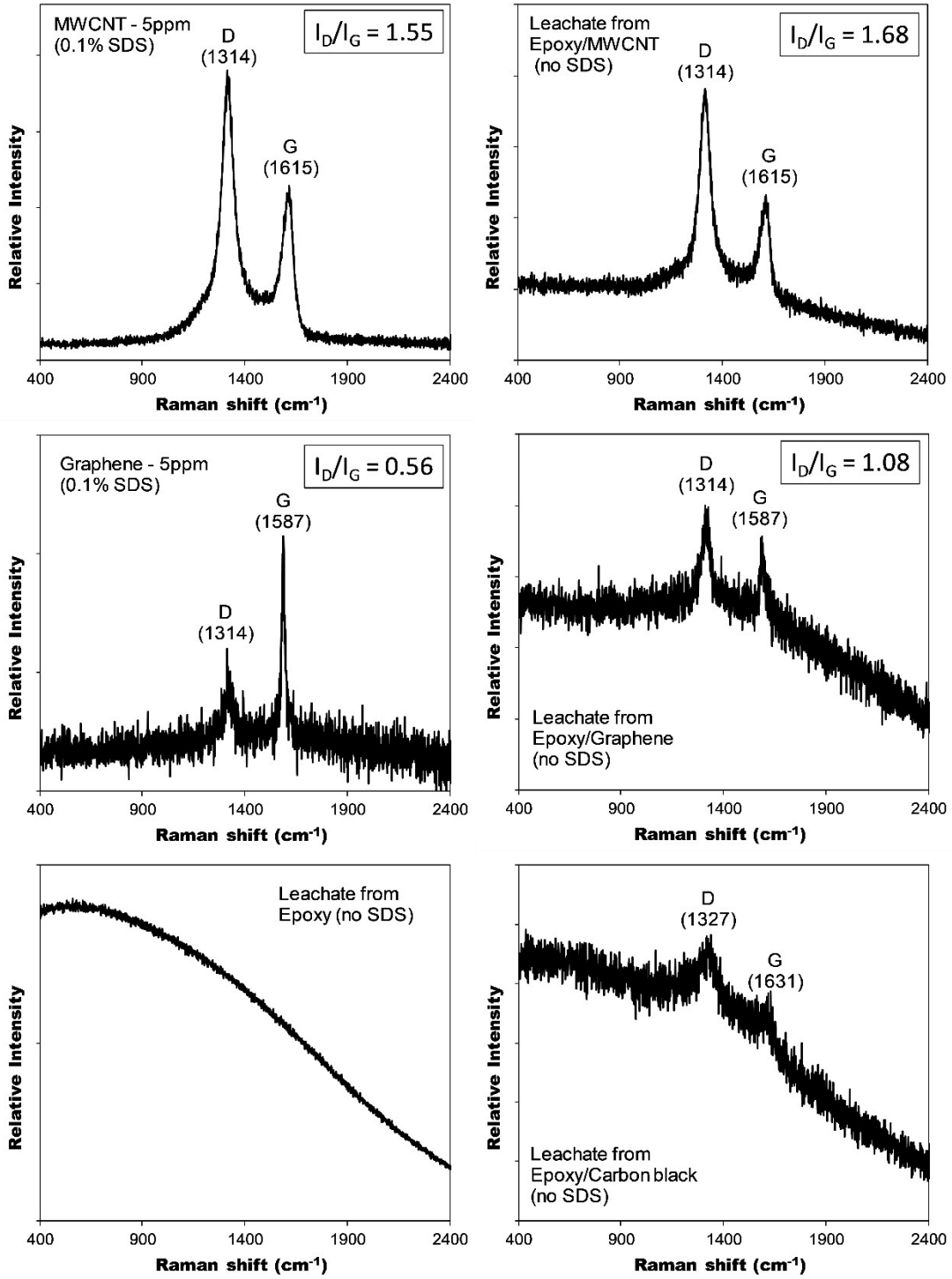

Figure S17. Raman spectra for selected Epoxy and Epoxy-ENM leachates with controls (left) and samples (right). The I_D/I_G ratio is shown in the top right corner of each plot, where applicable.

References

1. Walter, J.; Löhr, K.; Karabudak, E.; Reis, W.; Mikhael, J.; Peukert, W.; Wohlleben, W.; Cölfen, H., Multidimensional Analysis of Nanoparticles with Highly Disperse Properties Using Multiwavelength Analytical Ultracentrifugation. *ACS nano* **2014,** *8* (9), 8871-8886.

2. Mehn, D.; Rio-Echevarria, I. M.; Gilliland, D.; Kaiser, M.; Vilsmeier, K.; Schuck, P.; Wohlleben, W., Identification of nanomaterials: A validation report of two laboratories using analytical ultracentrifugation with fixed and ramped speed options. *NanoImpact* **2018,** *10*, 87-96.

3. Nguyen, T.; Petersen, E. J.; Pellegrin, B.; Gorham, J. M.; Lam, T.; Zhao, M.; Sung, L., Impact of UV irradiation on multiwall carbon nanotubes in nanocomposites: Formation of entangled surface layer and mechanisms of release resistance. *Carbon* **2017,** *116*, 191-200.

4. Ging, J.; Tejerina-Anton, R.; Ramakrishnan, G.; Nielsen, M.; Murphy, K.; Gorham, J. M.; Nguyen, T.; Orlov, A., Development of a conceptual framework for evaluation of nanomaterials release from nanocomposites: Environmental and toxicological implications. *Science of The Total Environment* **2014,** *473*, 9-19.

5. Petersen, E. J.; Lam, T.; Gorham, J. M.; Scott, K. C.; Long, C. J.; Stanley, D.; Sharma, R.; Alexander Liddle, J.; Pellegrin, B.; Nguyen, T., Methods to Assess the Impact of UV Irradiation on the Surface Chemistry and Structure of Multiwall Carbon Nanotube Epoxy Nanocomposites. *Carbon* **2014,** *69*, 194-205.

6. Nguyen, T.; Wohlleben, W.; Sung, L., Mechanisms of Aging and Release from Weathered Nanocomposites. In *Safety of Nanomaterials along Their Lifecycle: Release, Exposure, and Human Hazards*, Wohlleben, W.; Kuhlbusch, T.; Schnekenburger, J.; Lehr, C. M., Eds. CRC Press: 2014; pp 315-334.

7. Wohlleben, W.; Meyer, J.; Muller, J.; Muller, P.; Vilsmeier, K.; Stahlmecke, B.; Kuhlbusch, T. A. J., Release from nanomaterials during their use phase: combined mechanical and chemical stresses applied to simple and multi-filler nanocomposites mimicking wear of nano-reinforced tires. *Environmental Science: Nano* **2016,** *3*, 1036-1051.

8. Wohlleben, W.; Kingston, C.; Carter, J.; Sahle-Demessie, E.; Vázquez-Campos, S.; Acrey, B.; Chen, C.-Y.; Walton, E.; Egenolf, H.; Müller, P.; Zepp, R., NanoRelease: Pilot interlaboratory comparison of a weathering protocol applied to resilient and labile polymers with and without embedded carbon nanotubes. *Carbon* **2017,** *113*, 346-360.

9. Amin, M. U.; Scott, G., Photo-initiated oxidation of polyethylene effect of photo-sensitizers. *European Polymer Journal* **1974,** *10* (11), 1019-1028.

10. Chidambaram, M.; Krishnasamy, K., Drug-Drug/Drug-Excipient Compatibility Studies on Curcumin using Non-Thermal Methods. *Adv Pharm Bull* **2014,** *4* (3), 309-312.